Published in final edited form as:
Soft Matter. 2014 March 7; 10(9): 1356–1364. doi:10.1039/C3SM52518J.

Microgel Film Dynamics Modulate Cell Adhesion Behavior

Shalini Saxena[†,§], **Mark W. Spears Jr.**[§], **Hiroaki Yoshida**[§], **Jeffrey C. Gaulding**, **Andrés J. García**[‡,*], and **L. Andrew Lyon**[*]
School of Chemistry and Biochemistry and the Petit Institute for Bioengineering and Bioscience, Georgia Institute of Technology, Atlanta, GA 30332, USA

Abstract

A material's mechanical properties greatly control cell behavior at the cell-substrate interface. In this work, we demonstrate that microgel multilayers have unique elastic and viscoelastic-like properties that can be modulated to produce morphological changes in fibroblasts cultured on the film. Protein adsorption is also examined and the data are contrasted with the number of cells adhered. The dynamic interaction of cell and substrate is only partially explained by conventional understanding of surface-receptor interactions and substrate elasticity. Viscoelasticity, a mechanical property not often considered, plays a significant role at cellular length and time scales for microgel films.

Introduction

Cellular activity is known to be influenced by surrounding environmental factors.[1, 2, 3] For many years, researchers focused on the influence of bulk properties on cellular behavior such as elastic modulus.[4, 5, 6] More recently, investigators have realized the impact that length-scale has on the properties being investigated and have shifted primary focus from the macro-environment to the micro- or even nano-scale environment.[7] The fields of nanomaterials and nanotechnology have driven the technological innovations that have enabled this shift to take place. Advancements in nano-fabrication techniques have allowed more precision and detail both in construction and investigation of the cellular environment. For instance, nano-pillar arrays made with precise control over pillar position and flexibility allowed for collection of previously immeasurable cell traction forces.[8, 9] In another example, creation of a patterned elastomeric substrate allowed measurement of focal adhesion forces as the pattern was disrupted.[10] Other factors such as roughness[11] and chemical functionalization[12, 13] have also been designed into systems to exert greater control over cell behavior.

Biomaterials placed in physiological conditions immediately adsorb protein on the exposed surface soon followed by cell adherence.[14, 15] Cellular adherence is often correlated with the amount of protein and the nature of specific interactions with surface receptors. For example, the amount of adsorbed fibronectin on bioactive glass correlates with the strength of osteoblast adhesion to the surface.[16] Cell adhesion to a synthetic surface or a natural matrix is a complex process that involves integrin receptors in the cell membrane binding to surface-localized proteins. These proteins, such as fibronectin, may be produced by the cells

[*]Tel: 404-894-4090; lyon@gatech.edu. [*]Tel: 404-894-9384; andres.garcia@me.gatech.edu.
[†]School of Materials Science and Engineering, Georgia Institute of Technology, Atlanta, GA 30332, USA
[‡]George W. Woodruff School of Mechanical Engineering, Georgia Institute of Technology, Atlanta, GA 30332, USA
[§]Equally Contributing Authors

Electronic Supplementary Information (ESI) available. See DOI: 10.1039/b000000x/

as they seek to strengthen their adherence, adsorbed from the medium, or even built directly into the material in the case of designed biointerfaces.[13] Since cellular adhesion is critical in cell functions, substrates are often functionalized with ECM proteins or related peptides such as RGD to improve cell attachment.[15] Following ligand binding, integrins cluster together and recruit cytoskeletal and signaling components to form focal adhesions. These focal adhesion clusters are the primary way in which a cell interacts with its environment, providing feedback and mechanical cues about the surrounding material through the cell's cytoskeleton.[17]

Cells exert force on their surrounding environment as they attempt to probe the material properties through mechanosensing. Recent studies suggest that the primary mechanical property that controls cell adhesion and spreading is the elastic modulus, *E*.[18] Elasticity of the substrate can influence stem cell differentiation[19] and other cell functions such as movement[20] and nanoparticle uptake.[21] A cell can exert a significant amount of force on its surroundings. Munevar *et al.* measured the traction force of NIH3T3 fibroblasts on polyacrylamide substrates to be 3.03 $nN/\mu m^2$.[22] Galbraith and Sheetz measured the force exerted by an adhesive contact on a micro-machined silicon lever device to be approximately 3 nN.[23] Cells also have a characteristic appearance based on the modulus of the material that they are experiencing. "Hard" surfaces result in cell spreading and cytoskeletal organization, whereas "soft" surfaces result in rounded morphologies without the ability to form focal adhesions. In this context, "hard" surfaces are those having $E > 10kPa$, because above this approximate threshold, cells adhere strongly and show little variation in adhesion characteristics regardless of elastic modulus. However, below this threshold (which we will consider "biologically soft"), cells have extraordinary sensitivity to the material modulus.[24]

The elastic component of biomaterials has been broadly studied, because the elastic modulus of a material can often be altered without great synthetic effort. However, not as much attention has been paid to the viscous component of biomaterials. The questions of how biophysical forces are able to remodel a cell's surroundings or how movement of the surroundings is able to control cell behavior are largely unexplored. The difficulty in answering these questions lies primarily in selection and synthesis of a material with viscoelastic properties that respond to small forces on the time scale of cellular processes.

Microgels are discrete hydrogel particles that range in size from nanometers to a few microns that exhibit many of the same properties of hydrogels, but have the added benefit of responding to environmental changes on a faster time scale due to their size. Moreover, microgels have been used extensively as building blocks in the fabrication of thin films as either monolayers or layer-by-layer (LbL) multilayer films.[25,26]

We have previously shown that microgel LbL films have the ability to heal mechanically induced damage when sufficiently hydrated.[27, 28] This self-healing behavior is similar to other LbL polyelectrolyte systems that can recover from damage when exposed to water.[29] When linear strain is applied to a dry microgel film atop an elastomeric substrate, it plastically deforms, and when the strain is removed, the film relieves stress by wrinkling. After stretching, films are immersed in water to attempt to heal the damage and restore film integrity. During the healing process, films swell significantly, which requires rearrangement of film components that leads to recovery of as-prepared root mean square (RMS) roughness and surface morphology.[28] The self-healing process suggests that microgel films are dynamic materials that exhibit viscoelastic behavior on short time scales and small length scales.

Previous work in the Lyon group demonstrated the non-fouling nature of microgel films. The earliest studies assessed protein fouling and cell adhesion on 1 layer of poly(ethylene glycol diacrylate) (PEGDA) cross-linked microgels spin-coated onto glass. The amount of protein adsorption was low, with protein fouling decreasing as the length of the PEG cross-linker was increased. It was also found that microgel layers resisted cell attachment for several days, but surfaces not modified with PEGDA-containing microgels showed significant cell adhesion and proliferation.[30] A further study was conducted using the centrifugal deposition technique for building microgel films, which packs the particles tightly on the surface and ensures that no substrate is exposed. Four-layer microgel films strongly resisted cell attachment compared to glass or tissue culture polystyrene (TCP).[31] In addition, microgel-coated polyethylene terephthalate (PET) disks implanted in rats for 4 weeks resulted in a reduced inflammatory response relative to controls.[32] These successes prompted further study into the behavior of cells on microgel-modified substrates and exploration into the mechanism of adhesion resistance.

Given these previous studies, our growing knowledge of the dynamic nature of microgel multilayer films led us to investigate the properties of the film as a means of controlling cell adhesion. Salloum *et al*. have demonstrated alteration of vascular smooth muscle cell behavior by manipulating surface charge and hydrophobicity of polyelectrolyte multilayers (PEM's).[33] PEM's can be manipulated to affect cell adhesion and spreading by varying crosslinking amounts within the film[34] or by tuning film compliance through assembly at varying pH conditions.[35] Responsive microgel films have also been used in the thermally-triggered detachment of cells, taking advantage of the changes in microgel softness during swelling.[36] In principle, dynamic microgel multilayers also serve as intriguing substrates with which to study the effect of mechanical properties on cell behavior. For example, the rapid reorganization of the film components following perturbation (i.e. self-healing) could occur during cell attachment and spreading. This reorganization essentially represents a viscoelastic property of the film; the organization of the building blocks changes in response to an applied stress without a subsequent elastic recovery. Thus, we hypothesized that the viscoelasticity of microgel films could play a significant role in the process of cell attachment and spreading in a manner that differed from what might be predicted due to the film elasticity alone.

Experimental

Materials

All reagents were purchased from Sigma Aldrich (St Louis, MO) and used as received unless otherwise noted. The monomer *N*-isopropylacrylamide (NIPAm) was recrystallized from hexane (VWR International, West Chester, PA) and dried under vacuum before use. Reagents acrylic acid (AAc), *N*,*N*′-methylenebisacrylamide (BIS), poly(ethylene glycol) diacrylate (PEGDA) (Mw = 575 Da), sodium dodecyl sulfate (SDS), ammonium persulfate (APS), sodium phosphate, monobasic (NaH_2PO_4), sodium chloride, (3-aminopropyl)trimethoxysilane (APTMS), *N*-(3-dimethylaminopropyl)-*N*′-ethylcarbodiimide hydrochloride (EDC), and *N*-hydroxysuccinimide (NHS) were used as received. Poly(diallyldimethylammonium chloride) (pDADMAC) (Mw = 400–500 kDa) and branched polyethyleneimine (PEI) (typical Mw = 750 kDa) 50% w/w solution in water were both prepared as 0.1 mono M solutions in water. Water used in all reactions, particle purifications, and solution preparations was purified to a resistance of 18 M (Barnstead E-Pure System), and filtered through a 0.2 μm filter to remove particulate matter.

Microgel Synthesis

Microgels were synthesized as previously described.[37] The total monomer concentration was 100 mM with a molar composition of 66% NIPAm, 30% AAc, and either 4% PEGDA or 4% BIS. NIPAm, SDS, and either PEGDA or BIS were dissolved in water. The solution was added to a 3-neck round bottom flask and heated to 70 °C while purging with nitrogen and stirring for one hour. AAc was added 10 minutes prior to reaction initiation; 1 mL of APS solution in water was added to bring the total APS initiator concentration in the reaction to 1 mM, and the reaction was allowed to proceed for 4 hours. The reaction solution was removed from heat, allowed to cool, and filtered through glass wool. The microgels were purified by repeated sedimentation and resuspension in water. Finally, they were lyophilized for storage and resuspended as required in 10 mM, pH 7.4 PBS buffer with 100 mM NaCl ionic strength control.

Microgel Characterization

Diffusion coefficients were determined by dynamic light scattering (DLS) using a Protein Solutions DynaPro DLS (Wyatt Technology Corporation, Santa Barbara, CA) equipped with temperature control. Hydrodynamic radii (R_H) and polydispersities were calculated using Dynamics software for each particle type used in these experiments. All DLS measurements were carried out at 25 °C in either 10 mM PBS at pH 7.4 and 100 mM ionic strength or 10 mM formate buffer at pH 3.0 with 100 mM ionic strength to confirm incorporation of acid groups and pH responsivity (see Supporting Information).

Film Construction

Films for AFM force mapping and cell adhesion studies were assembled on amine-functionalized glass coverslips. To functionalize the surface, the substrates were shaken in 1% APTMS in absolute ethanol for 2 hours. After rinsing, the film was equilibrated in 10 mM pH 7.4 PBS with 100 mM NaCl ionic strength control for 30 minutes. The functionalized substrate was centrifuged at 2250 x g for 10 minutes in a 0.1 mg/mL microgel solution to deposit the first layer. All films had their first layer covalently adhered to the surface through EDC coupling. The film was equilibrated in 10 mM pH 5.5 MES buffer with 100 mM NaCl ionic strength control for 30 minutes, then transferred to a solution of 2 mM EDC / 5 mM NHS prepared in MES buffer and allowed to shake at room temperature for 2 hours. Film buildup then proceeded by rinsing with water and shaking in 0.1 mono M PEI (750 kDa) or pDADMAC (400–500 kDa) solution for 30 minutes. This process was repeated to a total of 4 layers of microgels with microgels being the final layer. The following film types were created:

PEGDA/pDADMAC: PEGDA-containing microgels identical in composition to those used in our previously published work[31] deposited via pDADMAC LbL assembly up to four layers.

BIS/pDADMAC: BIS-containing microgels deposited via pDADMAC LbL assembly up to four layers.

BIS/PEI: BIS-containing microgels deposited via PEI LbL assembly up to four layers.

PDMS Substrate Fabrication

Poly(dimethylsiloxane) (PDMS) substrates were prepared by mixing a 10:1 ratio by weight of elastomer to curing agent (Sylgard 184 Silicone Elastomer Kit, Dow Corning), degassing for 30 minutes, and curing at 50 °C for 24 hours. Cured PDMS was cut into 9 × 18 mm pieces, equilibrated in hexane for 2 hours, and again incubated at 50 °C in an oven for 2 hours to remove hexane. Pieces were stored in individual Eppendorf tubes filled with water until further use. Prior to use, the water was removed and replaced with 1.2 M HCl for

approximately sixteen hours. The pieces were then removed, washed 3 times with water, washed 2 times with absolute ethanol, and shaken in absolute ethanol for 30 minutes. Finally, the pieces were removed and placed in a separate solution of 1% APTMS in absolute ethanol for 2 hours while shaking. Once removed, the pieces were rinsed with water, at which point they were ready for LbL coating.

Film Cross-linking

In cases where the entire film was to be cross-linked, the coupling reaction was repeated after the film was completely assembled. The film was equilibrated in 10 mM pH 5.5 MES buffer with 100 mM NaCl ionic strength control for 30 minutes prior to cross-linking reaction. Films were then transferred to a solution of 8 mM EDC / 20 mM NHS prepared in MES buffer. The reaction was allowed to proceed for 2 hours at room temperature while shaking. After the cross-linking reaction, the films were rinsed with water and immersed in a 40 mM glycine solution in MES buffer for 2 hours to quench residual cross-linking reagents.

Film Stretching and Healing

Films were loaded into a custom-made stretching apparatus that allowed precise mechanical control over the degree of strain applied to the substrate. Coated PDMS substrates were clamped at both ends between glass plates connected to a micrometer- controlled, uniaxial translation stage. The film was parallel to the floor with the coated side up. Before applying a stress, the exposed film area was wet with distilled water for at least 1 minute to heal any damage associated with handling, dried with N_2, and measured along the stretching axis. After removal from the apparatus, brightfield microscopy images at 40X magnification were captured on an Olympus IX-70 inverted microscope equipped with a PixelFly black and white CCD camera.

Atomic Force Microscopy

We used Atomic Force Microscopy (AFM) force mapping to determine the elasticity of the microgel films. AFM has been used previously to probe the micro-environment elasticity of tissues and substrates in contact with cells, using a technique where the AFM tip is brought into contact with the surface to act as a nano-indenter.[38] Films were imaged and force mapped using an MFP-3D AFM from Asylum Research (Santa Barbara, CA). Images in air were collected in AC mode using silicon SPM probes with Al reflex coating, and a 42 N m^{-1} nominal force constant (Nanoworld, NCHR). Images in liquid were collected in contact mode using silicon nitride probes with Cr/Au reflex coating, and a 0.09 N m^{-1} nominal spring constant (Asylum, BL-TR400PB) mounted in the iDrive cantilever holder. All force curves were collected in contact mode. The samples were allowed to equilibrate in 10 mM, pH 7.4 PBS with 100 mM NaCl ionic strength control for approximately 30 minutes in the AFM chamber before analysis. Exact spring constants were determined on a clean glass coverslip by a combination of force curves and a thermal spectrum calibration using methods in the MFP-3D software. Force maps were collected as a 32 × 32 array of force curves with trigger point = 0.3 V. Elastic moduli were determined via the MFP-3D analysis tools using the Hertz model, assuming a Poisson ratio of 0.5 for the films, and assigning the appropriate tip geometry as a cone. Reported values were calculated by averaging all points from a force map on each of 3 separate samples and calculating a standard deviation for all points.

Protein Adsorption Assay

Human plasma fibronectin (FN, Mw: 400k – 500k, 500 μg/mL, Invitrogen) was coupled with Alexa Fluor® 488 succinimidyl ester (1 mg/mL, Molecular Probes) in 0.1M $NaHCO_3$ (pH 9.0, 100 μL) for 2 hours at room temperature. Unreacted fluorescent label was removed

by filtration and washing in PBS (pH 7.4) using Millipore (Billerica, MA) Amicon Ultra-15 centrifugal filtration units (3,000 MWCO). Fibronectin was recovered from the filter and the purified solution was diluted to approximately 2 ng/mL. The microgel films were immersed in 1 mL of the FN solution, kept for 24 hours at 37 °C, then washed with PBS three times. Fluorescence intensity of adsorbed FN was measured by a Biotek (Winooski, VT) Synergy H4 Multi-Mode Plate Reader. Films for stretching analysis after exposure to cell culture medium were treated according to the same procedure.

Cell Adhesion Assay

Microgel films were prepared in the same manner as above. The samples were washed with PBS 3 times and then immersed in 1 mL of Dulbecco's modified Eagle medium (DMEM) containing 10% fetal bovine serum (FBS). NIH3T3 fibroblast cells were seeded on the samples at the concentration of 2500 cells/cm^2 and cultured for 24 hours in a CO_2 incubator (37 °C, 5% CO_2). Cells attached to the microgel films were stained by incubation in 1 mL of PBS containing 2 mM of calcein-AM and 4 mM of ethidium homodimer (EthD-1) (LIVE/DEAD Viability/Cytotoxicity Assay, L3224, Molecular Probes) for 30 min at room temperature and imaged with a Nikon (Tokyo, Japan) Eclipse E400 fluorescence microscope. 20 images were recorded and analyzed from each of 3 samples. The number of attached cells was counted, and cell adhesion area was calculated in ImageJ for at least 200 cells per sample. For focal adhesion staining, vinculin was immunostained according to the following procedure: cells were permeabilized in cytoskeleton buffer (CSK), once in CSK (−) and twice in CSK (+) buffer [CSK(−): 3.02 mg/mL PIPES, 2.92 mg/mL NaCl, 0.61 mg/mL $MgCl_2$-$6H_2O$, and 51.3 mg/mL sucrose dissolved in water and adjusted to pH6.8; CSK(+): same as CSK (−) plus 1 mM phenylmethylsulfonyl fluoride, 1 μg/mL leupeptin, 1 μg/mL aprotinin, 1 μg/mL pepstatin, and 0.5% Triton X-100] then fixed in 4% paraformaldehyde, and blocked in 1% goat serum. Finally, they were incubated with monoclonal anti-vinculin antibody produced in mouse (V4505, Sigma-Aldrich) against vinculin followed by Alexa Fluor® 488 goat anti-mouse IgG (A11001, Molecular Probes), and gelled overnight for approximately 14 hours with Prolong® Gold antifade reagent with DAPI (Invitrogen).

Results and Discussion

The composition and tunable properties of these films allowed interrogation of the hypothesis that microgel film viscoelastic properties are a controlling factor in cell adhesion behavior. pDADMAC presents little opportunity for facile modification of covalent film connectivity, as it has no readily accessible reactive groups for conjugation. However, as seen in Figure 1, PEI is a highly branched polycation that similarly has many charged sites available for Coulombic interactions during the layer-by-layer buildup process. In addition, using PEI as the polycation introduces reactive amines into the film, enabling post-synthetic conjugation to the acid sites incorporated in the microgels. Films were either used as-prepared or the film mechanical properties were modulated by chemically cross-linking film components, thereby altering the elastic components as well as restricting the mobility of the components of the film. The cross-linking reaction bound free amines on PEI to carboxylic acid groups on themicrogels using EDC/NHS carbodiimide coupling, a common bioconjugation strategy (reaction scheme in supporting information). However, since pDADMAC does not contain primary amines (Figure 1), there are no opportunities for cross-linking reactions between the microgels and the polycation.

Monitoring the ability of four layer films to self-heal before and after cross-linking provided a simple method by which to demonstrate the effect of the cross-linking treatment on the microgel and polyelectrolyte mobility that is implied in the healing response, as well as provide evidence of changes in the film's mechanical properties. Films were assembled on

PDMS substrates and subjected to controlled linear strain. Figures 2 and 3 show that for all films, significant damage appeared with a wrinkling pattern lying perpendicular to the stretching axis. The damage pattern for BIS/pDADMAC and BIS/pDADMAC crosslink-treated films is a regular, repeating arrangement of parallel lines, in agreement with previous results.[28,39] However, the damage pattern in BIS/PEI films is more reminiscent of fractures on slightly different scales depending on whether the film has been crosslink-treated. For Figures 2c, 2f, and 3c the damage was no longer visible after healing in water, indicating a degree of microgel and polycation mobility in these films. However, the damage observed in the crosslink-treated BIS/PEI sample persisted even after the healing step. The lack of ability to self-heal once cross-linked demonstrates the importance of microgel and polycation mobility. Restriction of that mobility via covalent coupling severely limits the ability of the film to reorganize and heal. Furthermore, the difference in damage appearance suggests that the actual nature of the damage changes upon cross-linking, with the non-cross-linked films undergoing plastic deformation and wrinkling, while the cross-linked films likely crack due to a decrease in elasticity. Another way of viewing this is in terms of film viscoelasticity, where microgelfilms have viscoelasticity that responds on very short time scales, but the viscous component is removed by the cross-linking treatment. PEGDA/pDADMAC films are not included in these figures as their damage pattern closely resembles BIS/pDADMAC films and their healing characteristics have been amply demonstrated in previous work.[27]

There are differences between film types that are attributed to the polycation properties. The onset of damage is higher in BIS/PEI films (60% strain) relative to BIS/pDADMAC films (30% strain), suggesting that PEI-containing films have greater elasticity, possibly due to the very high molecular weight and branched nature of the polycation. We also found that films demonstrate essentially the same damage and healing behavior after exposure to cell culture medium (see Supporting Information).

Success of the cross-linking reaction and its effects on the film mechanics were also demonstrated by measuring the elastic properties of the films. Nanoindentation has been demonstrated as a powerful technique to determine the Young's modulus of a material. However, as microgel films exhibit heterogeneity across the surface and as they are composed of discrete building blocks, it is important to obtain an average modulus over a large area. Therefore, force mapping provides a mechanism to sample a large number of points within a film area in order to provide a high resolution picture of the film elasticity. The heterogeneity of elasticity at this length scale may also be important in obtaining an understanding of cellular interactions with a substrate at the length scale of cells and their focal adhesions.

AFM images of each film type were collected both in-air and in-liquid. Figure 4 shows height traces for all films including the crosslink-treated coatings. Importantly, four layers are sufficient to cover the surface and leave no exposed substrate. Even though identical BIS-containing microgels are used for BIS/pDADMAC and BIS/PEI films, the films have significant differences in appearance attributable to the polycation. BIS/pDADMAC films tend to be flat with little undulation, but BIS/PEI films have raised areas as evidenced by the darker areas in the images and the larger height bar scale with each image. Individual microgels are difficult to discern in BIS/PEI films, whereas they are relatively simple to discern in the BIS/pDADMAC films.

An increase in the number of physical or chemical cross-links within an acrylamide gel increases the stiffness of a material as exhibited through an increase in the Young's modulus.[24] All AFM force maps were 32 × 32 arrays of force indentation curves as displayed alongside the corresponding height traces in Figure 4. The Young's modulus was

determined for all film types as an average of all points within the array, and the results are shown in Figure 5. Force mapping was conducted in pH 7.4 PBS buffer, thereby mimicking the pH & ionic strength conditions experienced during the cell adhesion studies. As mentioned previously, above the threshold of approximately 10 kPa cells are able to adhere and show little preference or discrimination to the material modulus.[24] The uncross-linked BIS and PEI films used in this study have a modulus of approximately 100 kPa, an order of magnitude higher than the threshold value. The PEGDA/pDADMAC films are also above the threshold with a modulus of approximately 35 kPa. Thus, even the uncross-linked films should be stiff enough for cell adhesion to be favorable. When cross-linked, the Young's modulus of PEI films increases an additional order of magnitude to approximately 1 MPa. A small increase in stiffness is noted for the negative (BIS/pDADMAC) control after exposure to cross-linking reagents, but as noted above, the change is not sufficient to restrict self-healing and therefore does not appear to restrict microgel or polycation mobility. For each film type, multiple samples and multiple spots on a single sample were tested; intra-sample and inter-sample variability was low (see Supporting Information).

The modulus values reported may be thought of as "effective moduli." That is, the modulus value given may not be able to take microgel and polycation mobility into account, so the actual modulus of the film may be smaller than the measured value. The AFM tip used for force mapping has a diameter of 84 ± 24 nm and a height of 3.0 ± 0.5 μm. Thus, the tip samples a small portion of film surface area but may be expected to sample a significant amount of film thickness. Film modulus and film dynamics are closely inter-related properties. Once films have been fabricated, one property cannot be changed without influencing the other. In this investigation, the coupling reaction stiffens the film, causing both an increase in Young's modulus and eliminating the viscous component for the BIS/PEI films.

Protein Adsorption

Monolayers of BIS particles compared to PEGDA particles had been shown to allow increased protein adsorption and increased cell adhesion.[30] To ascertain the influence of protein adsorption on these microgel films, we measured the amount of fluorescent fibronectin(a common protein associated with cell binding) adsorbed into both one and four layer films with results displayed in Figure 6. In agreement with the previous studies,[30, 31] both a single layer of PEGDA-containing microgels and a single layer of BIS-containing microgels have low fluorescence intensity, corresponding to small amounts of adsorbed protein. Surprisingly, multilayer films have relatively high fluorescence intensity, indicating a high level of protein loading into the film. Even microgels incorporating PEGDA show very high protein loading when assembled into multilayers. BIS/PEI films, and the crosslink-treated BIS/PEI films in particular, adsorb a large amount of fibronectin, likely due to both the relatively large thickness of these films (see Figure S5) and the substantial excess charge within the film. When viewed independently of cell adhesion behavior, high protein loading into multilayer films is not a surprising result. Charged microgels adsorb large amounts of oppositely charged protein as demonstrated by loading of cytochrome c into AAc-containing microgels.[40] Also, in the film environment there are many excess charges on the polycation available for Coulombic interaction with proteins. We observe that multilayer films, which in previous studies displayed a strong resistance to cell attachment,[31] display the highest degree of protein ad/absorption. Thus, it appears that cell attachment does not correlate with protein fouling in the case of these particular films.

Cell Adhesion

Since the levels of protein adsorption achieved by the films suggested that PEGDA was not the key factor in preventing cell attachment, we next investigated whether our previous

observations regarding cell attachment to multilayers persisted in the novel film compositions of the present studies. Cell adhesion results and representative fluorescence images are displayed in Figure 7. Fibroblasts were stained with a LIVE/DEAD kit to assess cell viability after interaction with the film. Virtually all cells that adhered to the film remained alive. There is a degree of heterogeneity in the film which may contribute to areas with more cells adhered than others. However, a sufficient number of images were counted and averaged to obtain meaningful data over a wide film area. Quantitative results in Figure 7b (top)show that the one layer coatings exhibit high levels of cell attachment, but the corresponding four layer coatings have very few cells adhered. As noted above, cell adhesion is usually closely tied to the amount of protein on the surface, because cells interact with adsorbed proteins through specific receptors. Since the amount of protein adhered to four layer films is much higher than one layer films, it seems counterintuitive that the number of cells adhered follows the opposite trend. These data indicate that for uncross-linked microgel films, cell adhesion is not primarily controlled by the amount of protein on the surface, but is likely controlled by another film factor.

There is no statistical difference between the number of cells adhered on four layer BIS/pDADMAC and crosslink-treated BIS/pDADMAC films, indicating that the chemical change occurring during the cross-linking reaction is not affecting film properties or cell behavior. However, there is approximately a six-fold difference in the number of cells adhered to untreated and crosslink-treated BIS/PEI films, a change that we attribute both to the large change in Young's modulus and the restriction of microgel and polyelectrolyte mobility in these cross-linked films.

Further evidence for this hypothesis was obtained through examining cell morphology, and vinculin localization to focal adhesions. These two factors change dramatically on different film types and illustrate the cell interaction with the film. Representative images in Figure 7c show that cells are well spread on one layer films with recruitment of vinculin to focal adhesions at the cell periphery. One layer (that are covalently attached to the surface) films lack the mobile dynamics seen in multilayer films, thus cells sense favorable mechanical cues and are able to form focal adhesions. When the same cells are cultured on four layer films, cells are always round and are not able to spread on the surface. This finding suggests that, while the apparent modulus of the film is high enough that cells should adhere strongly, the cells are unable to form focal adhesions, likely because they are applying traction forces to a dynamic, reconfigurable interface. Once the BIS/PEI film is crosslink-treated, the cells once again are able to spread on the surface and show evidence of high vinculin concentration at the membrane periphery.

On the cross-linked films, a few cells were observed that were mostly rounded, indicating that the cross-linking treatment was not effective in that particular area of the surface or that there is some natural variation in fibroblast mechanosensing. This heterogeneity leads to no statistical difference in cell area on different substrates as seen in Figure 7b (bottom). The change in fibroblast morphology on uncross-linked and crosslink-treated films is striking, but it does not necessarily correlate with an equally stark difference in cell area.

Conclusions

A series of microgel films were constructed in order to examine the relationships between film mobility, protein adsorption, film mechanics, and fibroblast adhesion and spreading. Self-healing studies indicate that films wherein mobility of the microgels and polyelectrolyte is maintained are able to self-heal, while the cross-linked BIS/PEI films exhibit irreversible damage. AFM force mapping studies indicate that the Young's moduli of the films are all greater than 30kPa, suggesting that all of them should appear physiologically stiff. The

moduli increase with cross-linking, and cross-linked BIS/PEI films have the highest Young's modulus. Protein adsorption studies demonstrate that multilayer films adsorb large amounts of protein, regardless of incorporation of PEGDA. In contrast, fibroblast adhesion is minimal in uncross-linked multilayers, while the cells only display a spread morphology on the films with lowest microgel and polyelectrolyte mobility, the cross-linked BIS/PEI films and monolayer films. Thus, cell adhesion, cell morphology, and vinculin localization results cannot be explained based only on the basis of elasticity and protein adsorption. At the microscale, these intriguing results can potentially be attributed to the dynamic nature of these films, which are able to self-heal, unless covalently cross-linked. At the nanoscale, this is due to the viscoelastic characteristics of the microgels and the intervening polycation in the film context as they interact with fibroblasts, shifting beneath the cells as they try to form focal adhesions. Control over cellular adhesion by shifting of the material underneath the cell due to traction forces is, to our knowledge, one of the first demonstrations of viscoelastic material properties influencing cell behavior and attachment.

Supplementary Material

Refer to Web version on PubMed Central for supplementary material.

Acknowledgments

Funding for SS was provided by the NSF (2736B48) and the NSF Integrative Graduate Education and Research Traineeship program in Stem Cell Biomanufacturing (0965945). Funding for MWS was provided for by the Georgia Tech Center for Drug Design, Development and Delivery. Funding for HY was provided from the Japan Society for the Promotion of Science (JSPS) via a Postdoctoral Fellowship for Research Abroad. Funding for JCG was provided by the NIH (1 R01 GM088291-01) and the training grant: GTBioMAT Graduate Training for Rationally Designed, Integrative Biomaterials (T32 EB 006343), U.S. DOE GAANN award, the Georgia Tech Center for Drug Design, Development and Delivery, and the Georgia Tech TI:GER program. Additional funding for cell studies in the Garcia lab was provided by a grant from the NIH (R01 AR062920).

References

1. Boyan BD, Hummert TW, Dean DD, Schwartz Z. Biomaterials. 1996; 17:137–146. [PubMed: 8624390]
2. Lutolf MP, Hubbell JA. Nat Biotechnol. 2005; 23:47–55. [PubMed: 15637621]
3. Liu WF, Chen CS. Mater Today. 2005; 8:28–35.
4. Yeung T, Georges PC, Flanagan LA, Marg B, Ortiz M, Funaki M, Zahir N, Ming WY, Weaver V, Janmey PA. Cell Motil Cytoskel. 2005; 60:24–34.
5. Discher DE, Janmey P, Wang YL. Science. 2005; 310:1139–1143. [PubMed: 16293750]
6. Engler AJ, Sen S, Sweeney HL, Discher DE. Cell. 2006; 126:677–689. [PubMed: 16923388]
7. Bechtle S, Ang SF, Schneider GA. Biomaterials. 2010; 31:6378–6385. [PubMed: 20541256]
8. Kuo CW, Shiu JY, Chien FC, Tsai SM, Chueh DY, Chen PL. Electrophoresis. 2010; 31:3152–3158. [PubMed: 20803755]
9. Kuo CW, Chien FC, Shiu JY, Tsai SM, Chueh DY, Hsiao YS, Yang ZH, Chen PL. Nanotechnology. 2011:22.
10. Balaban NQ, Schwarz US, Riveline D, Goichberg P, Tzur G, Sabanay I, Mahalu D, Safran S, Bershadsky A, Addadi L, Geiger B. Nat Cell Biol. 2001; 3:466–472. [PubMed: 11331874]
11. Chung TW, Liu DZ, Wang SY, Wang SS. Biomaterials. 2003; 24:4655–4661. [PubMed: 12951008]
12. Hersel U, Dahmen C, Kessler H. Biomaterials. 2003; 24:4385–4415. [PubMed: 12922151]
13. Keselowsky BG, Collard DM, Garcia AJ. Proc Natl Acad Sci U S A. 2005; 102:5953–5957. [PubMed: 15827122]
14. Schakenraad JM, Busscher HJ. Colloid Surface. 1989; 42:331–343.
15. Rahmany MB, Van Dyke M. Acta Biomater. 2013; 9:5431–5437. [PubMed: 23178862]

16. Garcia AJ, Ducheyne P, Boettiger D. J Biomed Mater Res. 1998; 40:48–56. [PubMed: 9511098]
17. Geiger B, Spatz JP, Bershadsky AD. Nat Rev Mol Cell Bio. 2009; 10:21–33. [PubMed: 19197329]
18. Michael KE, Garcia AJ. Method Cell Biol. 2007; 83:329.
19. Higuchi A, Ling QD, Chang Y, Hsu ST, Umezawa A. Chem Rev. 2013; 113:3297–3328. [PubMed: 23391258]
20. Lo CM, Wang HB, Dembo M, Wang YL. Biophys J. 2000; 79:144–152. [PubMed: 10866943]
21. Huang CJ, Butler PJ, Tong S, Muddana HS, Bao G, Zhang SL. Nano Lett. 2013; 13:1611–1615. [PubMed: 23484640]
22. Munevar S, Wang YL, Dembo M. Biophys J. 2001; 80:1744–1757. [PubMed: 11259288]
23. Galbraith CG, Sheetz MP. Proc Natl Acad Sci U S A. 1997; 94:9114–9118. [PubMed: 9256444]
24. Rehfeldt F, Engler AJ, Eckhardt A, Ahmed F, Discher DE. Adv Drug Deliver Rev. 2007; 59:1329–1339.
25. Guan Y, Zhang Y. Soft Matter. 2011; 7:6375–6384.
26. Wong JE, Gaharwar AK, Mueller-Schulte D, Bahadur D, Richtering W. Journal of Magnetism and Magnetic Materials. 2007; 311:219–223.
27. South AB, Lyon LA. Angewandte Chemie International Edition. 2010; 49:767–771.
28. Gaulding JC, Spears MW, Lyon LA. Polymer Chemistry. 2013; 4:4890–4896. [PubMed: 24443657]
29. Li Y, Wang X, Sun JQ. Chem Soc Rev. 2012; 41:5998–6009. [PubMed: 22797079]
30. Nolan CM, Reyes CD, Debord JD, Garcia AJ, Lyon LA. Biomacromolecules. 2005; 6:2032–2039. [PubMed: 16004442]
31. South AB, Whitmire RE, Garcia AJ, Lyon LA. ACS Appl Mater Interfaces. 2009; 1:2747–2754. [PubMed: 20356152]
32. Bridges AW, Singh N, Burns KL, Babensee JE, Lyon LA, Garcia AJ. Biomaterials. 2008; 29:4605–4615. [PubMed: 18804859]
33. Salloum DS, Olenych SG, Keller TCS, Schlenoff JB. Biomacromolecules. 2005; 6:161–167. [PubMed: 15638516]
34. Schneider A, Francius G, Obeid R, Schwinte P, Hemmerle J, Frisch B, Schaaf P, Voegel JC, Senger B, Picart C. Langmuir. 2006; 22:1193–1200. [PubMed: 16430283]
35. Thompson MT, Berg MC, Tobias IS, Rubner MF, Van Vliet KJ. Biomaterials. 2005; 26:6836–6845. [PubMed: 15972236]
36. Schmidt S, Zeiser M, Hellweg T, Duschl C, Fery A, Möhwald H. Adv Funct Mat. 2010; 20:3235–3243.
37. Hendrickson GR, Smith MH, South AB, Lyon LA. Adv Funct Mat. 2010; 20:1697–1712.
38. Domke J, Radmacher M. Langmuir. 1998; 14:3320–3325.
39. Park CW, South AB, Hu XB, Verdes C, Kim JD, Lyon LA. Colloid Polym Sci. 2011; 289:583–590.
40. Smith MH, Lyon LA. Macromolecules. 2011; 44:8154–8160. [PubMed: 22058574]

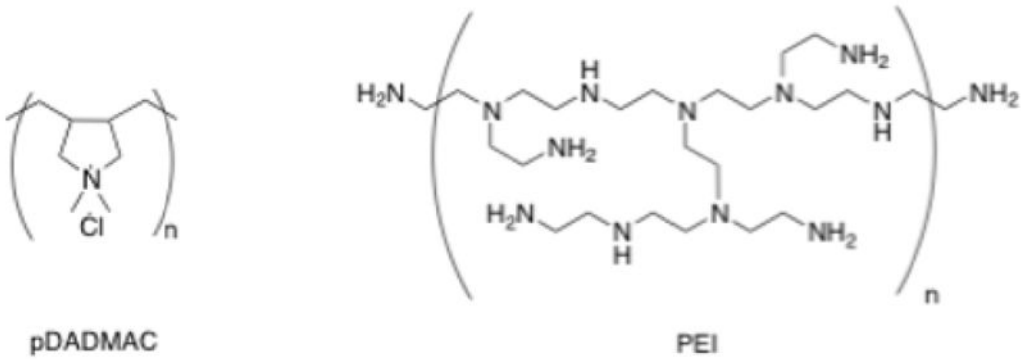

Figure 1.
Chemical structures of the polycations used for film assembly.

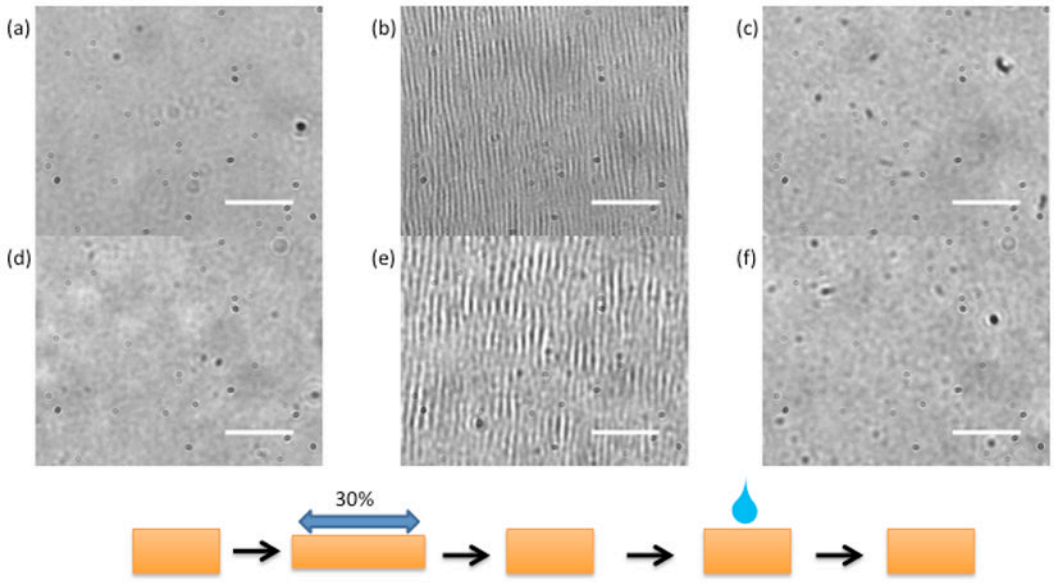

Figure 2.
Brightfield microscopy images of BIS/pDADMAC four layer films. (a–c) untreated (d–f) crosslink-treated. (a, d) before damage (b, e) after 30% linear strain applied (c, f) healed with water after damage. All BIS/pDADMAC films self-heal. Scale bars are 30 μm.

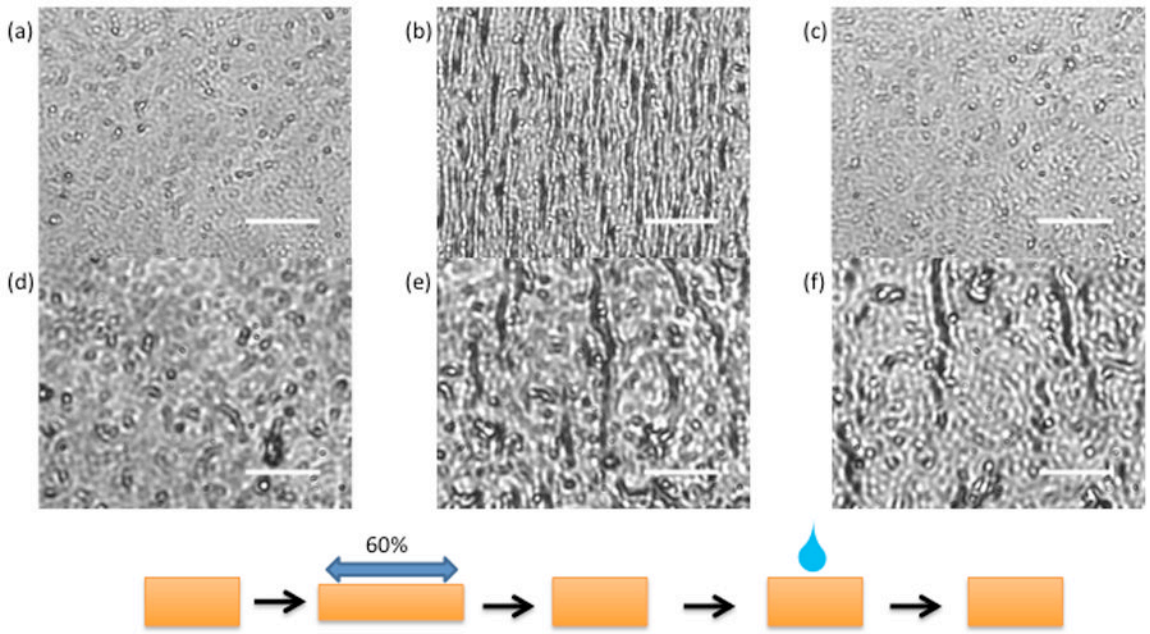

Figure 3.
Brightfield microscopy images of BIS/PEI four layer films. (a–c) untreated (d–f) crosslink-treated. (a, d) before damage (b, e) after 60% linear strain applied (c, f) healed with water after damage. Crosslink-treated BIS/PEI films do not self-heal. Scale bars are 30 μm.

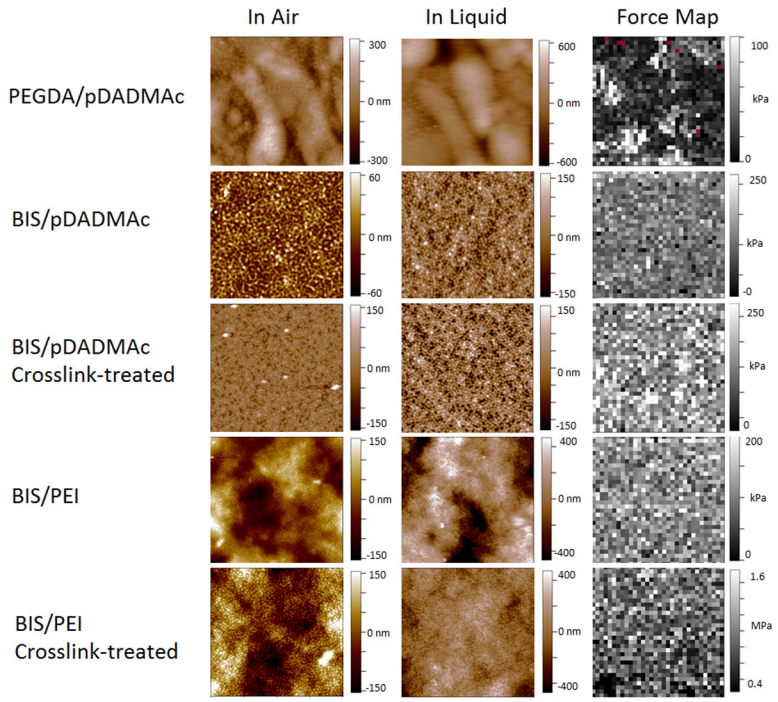

Figure 4.

AFM height traces and force maps for films used in this study. All force maps were collected in PBS buffer. Height scales and modulus scales are kept constant where appropriate. All images and force maps were collected at 20°C. All images and force maps are 20 × 20 μm.

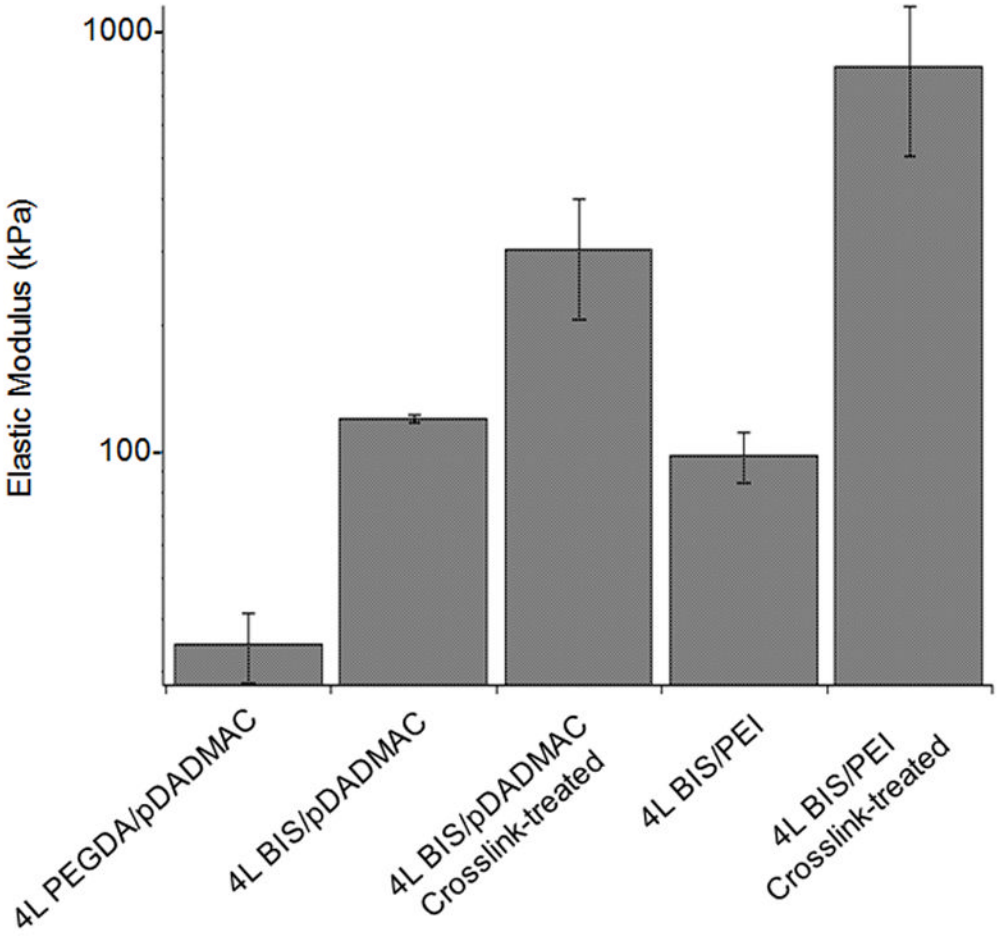

Figure 5.
Graph of AFM force mapping results. Error bars are standard deviations; n=3 for each film type. BIS/pDADMAC untreated vs. BIS/pDADMAC crosslink-treated, p = 0.012; BIS/PEI untreated vs. BIS/PEI crosslink-treated, p = 0.017

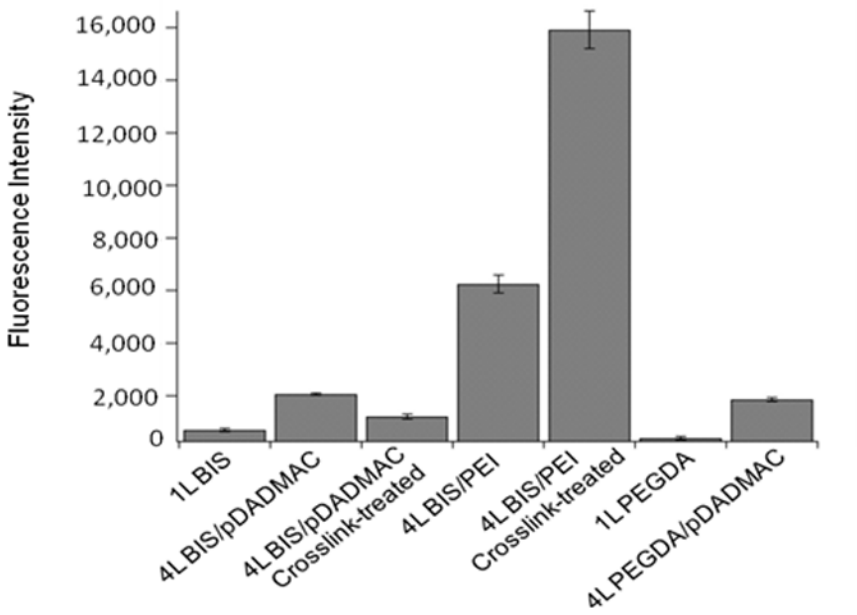

Figure 6.
Fluorescence intensity values for fluorescent fibronectin adsorbed into microgel films at 37°C. Error bars are standard deviations. Results are statistically significant with all $p < 0.0045$ (n=3).

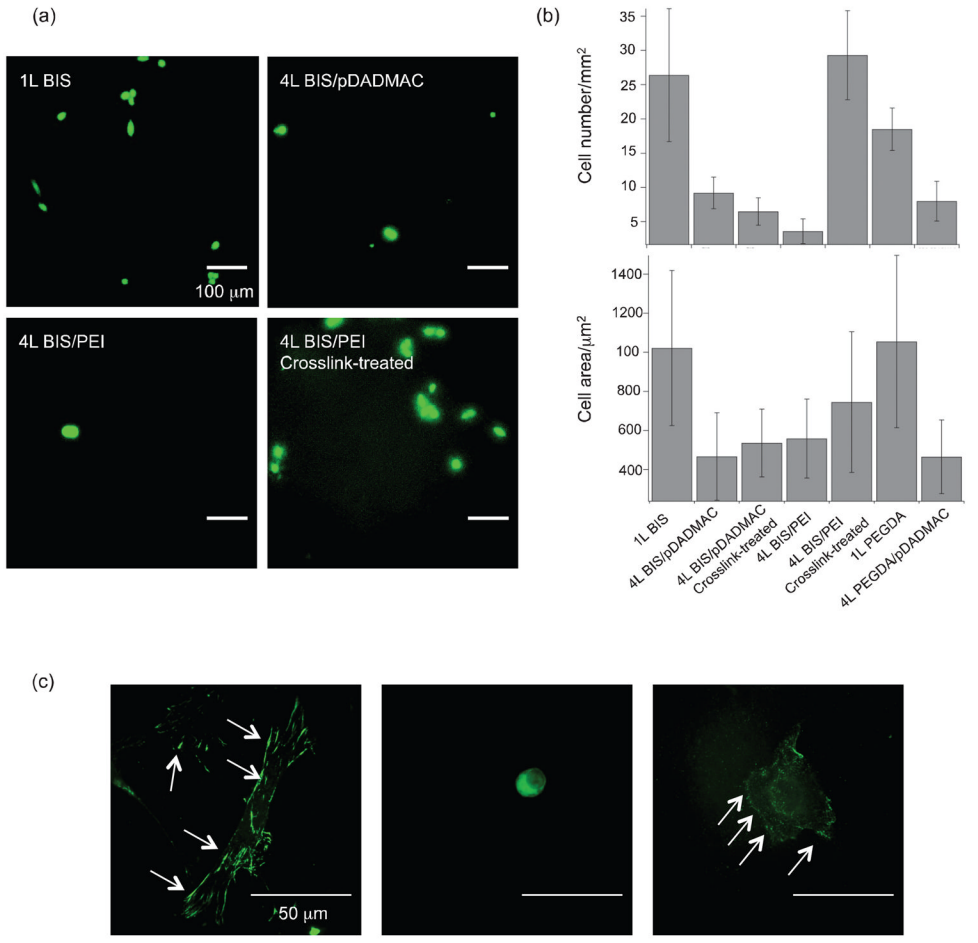

Figure 7.

Fibroblast adhesion on microgel films after 24h culture at 37°C. (a) Representative images of LIVE/DEAD staining of cells on various films; scale bar = 100 μm (b) (upper panel) The number of cells adhered on the films analyzed from LIVE/DEAD images; 4L BIS/pDADMAC vs. 4L crosslink-treated BIS/pDADMAC, $p=0.206$; all others $p<0.04$(lower panel) Area of adhered cells analyzed from LIVE/DEAD images; all $p>0.1$ (c) Vinculin expression of fibroblasts cultured on various films; 1L BIS (left), 4L untreated BIS/PEI (middle), and 4L crosslink-treated BIS/PEI (right). Arrows in images indicate vinculin staining; scale bar = 50 μm.